IOP Publishing Semiconductor Science and Technology
Semicond. Sci. Technol. **35** (2020) 125025 (9pp) https://doi.org/10.1088/1361-6641/abb71d

Growth of GaN on monolayer hexagonal boron nitride by chemical vapor deposition for ultraviolet photodetectors

Wenhui Zhu[1], Jiawei Si[1], Lei Zhang[1], Tao Li[1], Wenqing Song[1], Yuting Zhou[2], Jiahao Yu[3], Rui Chen[3], Yexin Feng[2] and Liancheng Wang[1]

[1] State Key Laboratory of High Performance Complex Manufacturing, College of Mechanical and Electrical Engineering, Central South University, Changsha, Hunan 410083, People's Republic of China
[2] Hunan Provincial Key Laboratory of Low-Dimensional Structural Physics and Devices, School of Physics and Electronics, Hunan University, Changsha, Hunan 410082, People's Republic of China
[3] Department of Electrical & Electronic Engineering, Southern University of Science and Technology, Shenzhen, Guangdong 518055, People's Republic of China

E-mail: liancheng_wang@csu.edu.cn and zhangl207@csu.edu.cn

Received 17 May 2020, revised 28 July 2020
Accepted for publication 10 September 2020
Published 27 October 2020

Abstract

Chemical vapor deposition (CVD) technology is a simple and flexible method used to prepare high-quality crystalline materials. Traditional CVD technology, based on pre-deposited thin catalyst metal, usually produces nanostructures instead of continuous films. In this work, a continuous GaN film on a monolayer boron nitride (h-BN) insertion layer is demonstrated using CVD technology. The experimental results and theoretical calculations indicate that abundant GaN nanocrystallites are firstly formed at the edges or grain boundaries of the monolayer h-BN by quasi-van der Waals epitaxy. Then, the vapor-solid mechanism will control further growth of the GaN nanocrystallites, causing them to merge into a continuous GaN film. Meanwhile, the CVD-grown GaN ultraviolet detector exhibits a relatively high responsivity with a value of 0.57 A W^{-1} at 2 V. In this paper, a simple low-cost CVD method is proposed for preparing continuous films on two-dimensional materials for electronic and optoelectronic devices.

Supplementary material for this article is available online

Keywords: gallium nitride, chemical vapor deposition, hexagonal boron nitride, nanocrystalline, ultraviolet photodetector

(Some figures may appear in colour only in the online journal)

1. Introduction

Gallium nitride (GaN), with a wide direct bandgap (3.4 eV), is an important type of semiconductor material for high-powered devices and optoelectronic devices, such as metal semiconductor field effect transistors, high electron mobility transistors, photodetectors (PDs), and light-emitting diodes (LEDs), due to its high carrier mobility, fast radiative recombination rates, as well as its long-term stability and reliability [1–7]. Several methods have been used to realize heteroepitaxy in GaN films, including metal—organic chemical vapor deposition (MOCVD) [6], molecular beam epitaxy (MBE) [2], and hydride vapor phase epitaxy (HVPE) [8, 9]. In contrast, chemical vapor deposition (CVD) technology is an economical method with a relatively simple experimental procedure and a high growth yield [10, 11]. The preparation of low-cost continuous GaN films by the CVD method is of great significance. However, most CVD-grown GaN utilizes a catalytic mechanism, using a pre-deposited thin metal layer as the catalyst, which can result in the generation of GaN nanostructures,

including nanowires, nanotubes, and nanobelts [12–14]. This limits the application of CVD-GaN film materials.

Recently, the exotic properties of layered two-dimensional (2D) materials have attracted much attention, and they are widely applied in the epitaxy of III-nitride films. This new approach of III-nitrides deposited on 2D-layered materials is called quasi-van der Waals epitaxy (QvdWE) [15–17]. Many 2D materials such as graphene, hexagonal boron nitride (h-BN), and MoS_2 have been considered for use as a buffer layer to improve the epitaxial quality of III-nitrides [6, 18–21]. Chen *et al* demonstrated the growth of AlN on sapphire substrates using a graphene interlayer treated by an N_2 plasma to make high-performance deep ultraviolet light-emitting diodes by MOCVD [21]. Iwan Susanto *et al* have successfully grown GaN thin films by plasma-assisted molecular beam epitaxy (PAMBE) on 2D MoS_2 layers [19]. It has been proved that III-nitride epitaxy on 2D materials has made great progress and it is successfully applied in some equipment including MOCVD, MBE, and HVPE. In addition, 2D materials can relax the strict requirements for lattice matching of conventional heteroepitaxy utilizing the QvdWE method [6, 9, 21 –25]. Thus, this suggests a potential approach for preparing continuous GaN films on 2D materials in a simple manner by utilizing the CVD method.

In this paper, the growth of continuous GaN films has been successfully realized by the CVD method using 2D materials as the intermediate buffer layer. Herein, h-BN is chosen for GaN epitaxy due to its wurtzite crystal structure and lattice constant. Furthermore, a PD based on CVD-grown GaN film has been fabricated that exhibited satisfactory ultraviolet (UV) detection performance.

2. Experimental section

2.1. Synthesis and transfer process of h-BN film

Monolayer h-BN was synthesized on polished copper foil (Cu (111)) by CVD. Polymethyl methacrylate (PMMA) was then spun as a transfer medium and coated on the h-BN/Cu (111), and subsequently baked at 100 °C for 25 min. Following that, the PMMA/h-BN/Cu (111) stack was dipped into a $FeCl_3$ solution until the copper foil was etched completely. The floating h-BN covered by PMMA was transferred to deionized water for profuse rinsing and then transferred to the sapphire. Finally, the PMMA/h-BN/sapphire structure was sequentially cleaned by acetone, ethyl alcohol, and deionized water, followed by a high-temperature cleaning process in a reducing (H_2) atmosphere to remove the PMMA layer thoroughly. A schematic diagram of the h-BN transfer process from the Cu (111) to the sapphire substrate is shown in figure S1 (available online at stacks.iop.org/SST/35/125025/mmedia) (supporting information).

2.2. Preparation of GaN film and fabrication of GaN photodetector

GaN film was prepared on the h-BN film by a simple CVD process, as illustrated in figure S1 (supporting information). Ga_2O_3 powder and NH_3 gas were introduced as the precursors of gallium (Ga) and nitrogen (N), respectively. The reaction was carried out in an alundum tube inserted in a horizontal single-zone CVD tubular furnace. Ga_2O_3 powder (0.5 g) was placed in an alundum boat, and the h-BN/sapphire substrate was placed at a distance of about 3 cm from the Ga source. Before the reaction, the alundum tube was pumped out to maintain a pressure of 10^{-3} Pa. The substrate was then heated to 1200 °C at a rate of 10 °C min^{-1} with N_2 shielding gas. Following that, the N_2 was removed and NH_3 was added to the tube at a flow rate of 200 sccm, then the system was maintained for different growth times. After that, the NH_3 was replaced by N_2 (50 sccm), and growth was halted by cooling to room temperature. The GaN film with a growth time of 150 min was used to fabricate the PD. Interdigital electrodes were constructed on the GaN film by conventional UV-lithography and lift-off technology with a finger width and spacing of 10 μm. About 30 nm Ni was deposited on top of the GaN film to complete the fabrication of the PD using magnetron sputtering.

2.3. Computational model

In this study, the adsorption energies of Ga atoms at the edge and the basal plane of a single-layer BN sheet were calculated using the Vienna *ab initio* simulation package based on density functional theory (DFT) [26]. The Perdew–Burke–Ernzerhof function with a generalized gradient approximation was used to optimize the atomic structures and calculate the total energies of various adsorption geometries [27]. Projector-augmented wave potentials were used with a cutoff energy of 600 eV. The BN plane was set to the X–Y plane, while the Z-axis was selected as the normal direction. Regarding the adsorption of Ga atoms on the BN-zigzag (armchair) edge, an h-BN supercell with a 4×3 surface was the periodicity used with a $2 \times 1 \times 2$ ($1 \times 2 \times 2$) k-point mesh. All atoms were allowed to relax until the force acting on the atoms was less than 0.03 eV $Å^{-1}$.

3. Results and discussions

A structural diagram and a photo of GaN/h-BN/sapphire are shown in figure 1(a). It should be noted that the GaN material can only be found on the monolayer h-BN (the right side of figure 1(a)). Typical hexagonal nanostructures about 1 μm in thickness (inset of figure 1(b)) can be observed for the 10 min CVD growth time in the scanning electron microscopy (SEM) images in figures 1(b) and S2 (supporting information). Similar structures are obtained when the growth time is less than 10 min (1 min, 2 min, 5 min, 10 min). Analysis using an energy dispersive spectrometer (EDS) shows that the atomic percentages are 53% (N) and 47% (Ga) in figure S3 (supporting information), respectively. The typical hexagonal crystal features and the EDS results indicate that the nanostructures are GaN islands. The sizes and densities of the GaN islands are summarized in figures 1(g) and (h), respectively. For the 10 min-grown GaN islands (the inset of figure 1(g)),

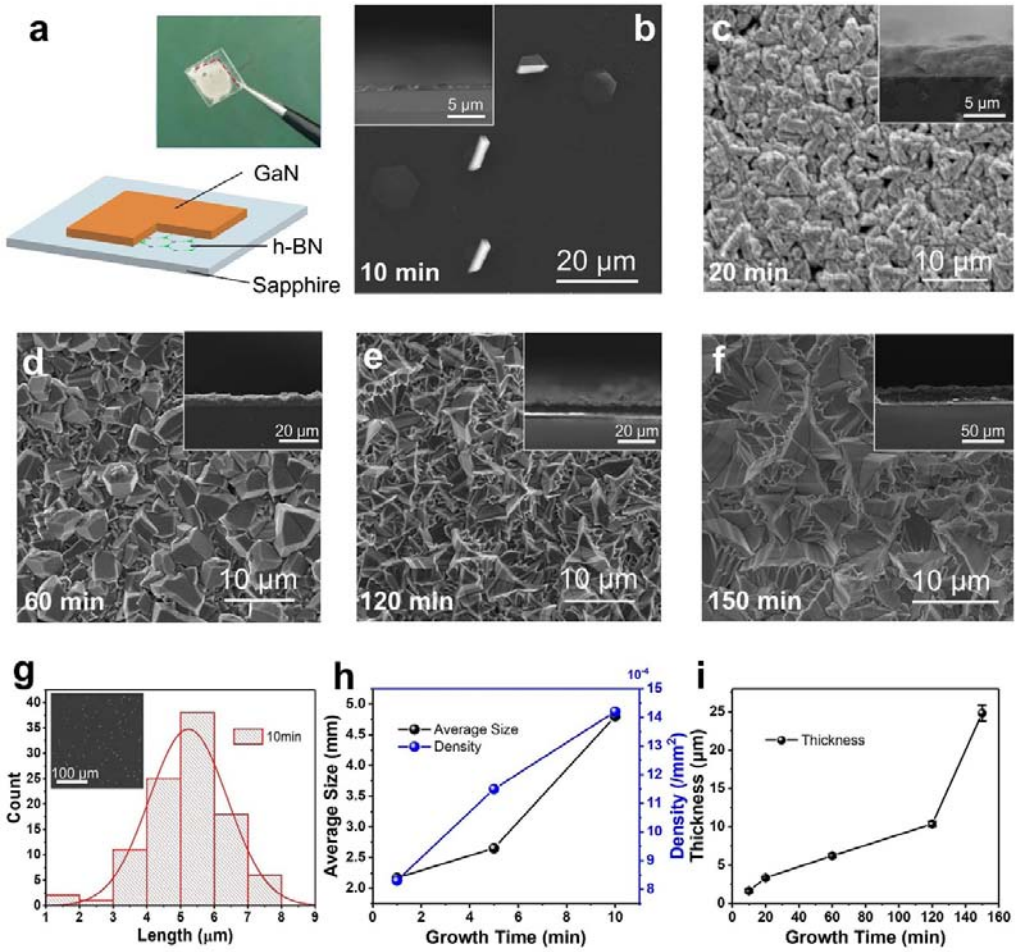

Figure 1. Characterization of epitaxial growth GaN islands and films made by CVD on an h-BN/sapphire substrate. (a) structural diagram and photograph of GaN/h-BN/sapphire. Different morphologies of GaN islands and films on monolayer h-BN with growth times of: 10 min (b), 20 min (c), 60 min (d), 120 min (e), 150 min (f), respectively. The insets of (b-f) show the corresponding cross-section images made by SEM. (g) Statistical diagram and SEM diagram of the GaN islands' size distribution with a 10 min growth time. (h) GaN islands' average size and density versus growth time. (i) Variation of GaN layer thickness with growth time.

the sizes range from about 1 μm–8 μm, and present a standard Gaussian distribution. The average sizes and densities of the GaN islands gradually increase with growth time, as shown in figure 1(h). Once the growth time exceeds 20 min, a continuous GaN film will form. Different morphologies of GaN films can be observed in figures 1(c–f) with increasing growth times. The film thicknesses increase from 3.4 μm to 24 μm, as shown in the insets of figures 1(c–f). Figure 1(i) illustrates the film thickness with varying growth times, and the growth rate of the GaN film is calculated to be 0.16 μm min^{-1}.

An x-ray diffractometer (XRD) spectrum of θ to 2θ scans of a 10 min-grown GaN/h-BN/sapphire structure is shown in figure 2(a). Three wurtzite crystal peaks are observed, corresponding to GaN (002), (101), (004) facets at 34.61°, 36.89°, 72.96°, respectively. An Al_2O_3 (006) peak from the sapphire substrate appears, and no h-BN peak signature is observed, which can be explained by the monolayer h-BN structure. The XRD results of GaN films with different growth times show similar characteristic peaks (figure S4). The statistical results of the full width at half maximum (FWHM) of the CVD-grown GaN film are shown in the inset of figure 2(a). FWHMs of the (002) and (101) facets gradually decrease from 0.3° to 0.22° and from 0.26° to 0.19°, respectively, improving the crystal quality with growth time. The crystallinity of the GaN islands was further studied by high-resolution transmission electron microscopy (HRTEM) in figure 2(b). The interplanar distance is 0.276 nm, corresponding to the (100) and (010) crystal planes with an angle of 60°, which confirms the hexagonal wurtzite GaN structure. The electron diffraction pattern of the GaN islands (inset of figure 2(b)) confirms its monocrystal characteristics. The composite GaN/h-BN heterostructure is characterized by Raman microspectroscopy using a 785 nm laser at room temperature. Figure 2(c) shows the Raman spectroscopy of a 10 min-grown GaN nanocrystallite on an h-BN/sapphire substrate, and its inset is the Raman spectroscopy of the h-BN/sapphire substrate. The Raman peak located at 1372 cm^{-1} corresponding to the standard h-BN E_{2g} vibration mode can be observed in the GaN/h-BN/sapphire and h-BN/sapphire structures, revealing the existence of an h-BN film after GaN growth. Meanwhile,

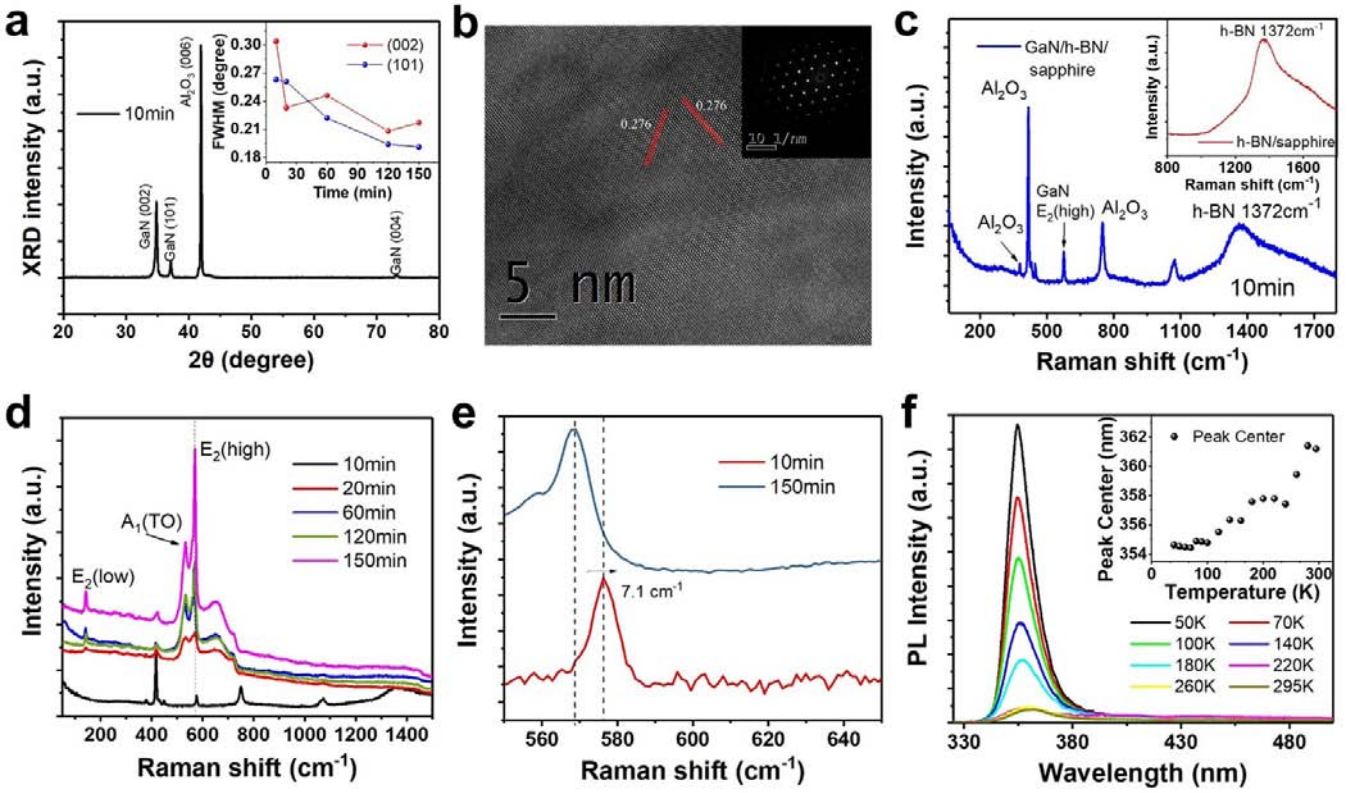

Figure 2. XRD, TEM, Raman and PL analysis of GaN islands and films. (a) XRD θ *to* 2θ scans of GaN islands with a 10 min-grown time. The FWHM statistical results for (002) and (101) with different growth times are shown in the inset. (b) HRTEM and electron diffraction pattern of GaN nanocrystallite. (c) Raman spectra of GaN/h-BN/sapphire. The inset shows the Raman spectra of h-BN/sapphire. (d) Raman spectra of GaN layers with different growth times. (e) Comparison of the Raman peaks of 10 min-grown GaN nanocrystallite and 150 min-grown GaN film. (f) PL spectra of 150 min-grown GaN film at different temperatures. The inset shows a plot of PL peak center versus temperature.

a peak located at 576.1 cm^{-1} can distinctly be detected in the GaN/h-BN/sapphire structure, which belongs to the $E_2{}^{high}$ model of hexagonal wurtzite GaN. These results prove the coexistence of wurtzite GaN and h-BN after CVD growth. GaN Raman spectroscopies with varied growth times are shown in figure 2(d). The peak intensity of the $E_2{}^{high}$ mode gradually increases, indicating improved crystallinity with increasing GaN film thickness. In addition, the $E_2{}^{high}$ peak of 150 min-grown GaN film is located at 569 cm^{-1}, which is consistent with the reported standard value. The $E_2{}^{high}$ peak of the 10 min-grown GaN nanocrystallite exhibits an obvious red shift up to 7.1 cm^{-1}, as shown in figure 2(e). Studies have indicated that the $E_2{}^{high}$ mode of GaN is sensitive to stress [28, 29]. Although monolayer h-BN enables GaN epitaxial growth, it cannot eliminate the lattice and thermal mismatch between h-BN and GaN, resulting in interfacial stress and a redshift of the Raman peak. For the 150 min-grown GaN layer, the thicker film can mitigate the stress effect originating from the interface, effectively improving the crystallinity. Figure 2(f) shows the temperature-dependent photoluminescence (PL) spectra of 150 min-grown GaN film from 50 K to 295 K excited by a 325 nm He-Cd laser. A filter for removing the yellow luminescence band was used. A dominant peak located at 361.2 nm is observed at 295 K, corresponding to the near band-edge (NBE) emission of wurtzite GaN. Meanwhile, the PL intensity gradually decreases with increasing measurement temperature, due to enhanced non-radiative recombination [30]. In addition, the GaN NBE emission peak exhibits a 6.6 nm red shift from 354.6 nm at 50 K to 361.2 nm at 295 K (inset of figure 2(f)). Apart from this, it is found the NBE peak (361.2 nm at 295 K) is below the previously reported figure for wurtzite GaN (about 364 nm). The shift in the NBE peak indicates the stress in the GaN material, which is probably associated with crystal intrinsic defects in the growth process [31, 32]. These results indicate the satisfactory optical quality of the GaN film, which makes our process a potential approach for the fabrication of optoelectronic devices.

To study the GaN growth mechanism, GaN was grown on unincorporated equilateral-triangle-shaped monocrystalline h-BN with a crystal size of about 8.5 μm, as shown in figure 3(a), at 1200 °C for 1 min by CVD. Some nanocrystallites can be observed on the edge of trianglular h-BN, as shown by SEM in figure 3(b). The nanocrystallites are of various shapes, and their average size is about 2.3 μm (inset of figure 3(b)). Figure 3(c) shows the EDS mapping of the Ga element corresponding to figure 3(b). It can be seen that the Ga element is mostly located at the sites where nanocrystallites exist. Figure 3(d) shows the atomic force microscopy (AFM) characterization

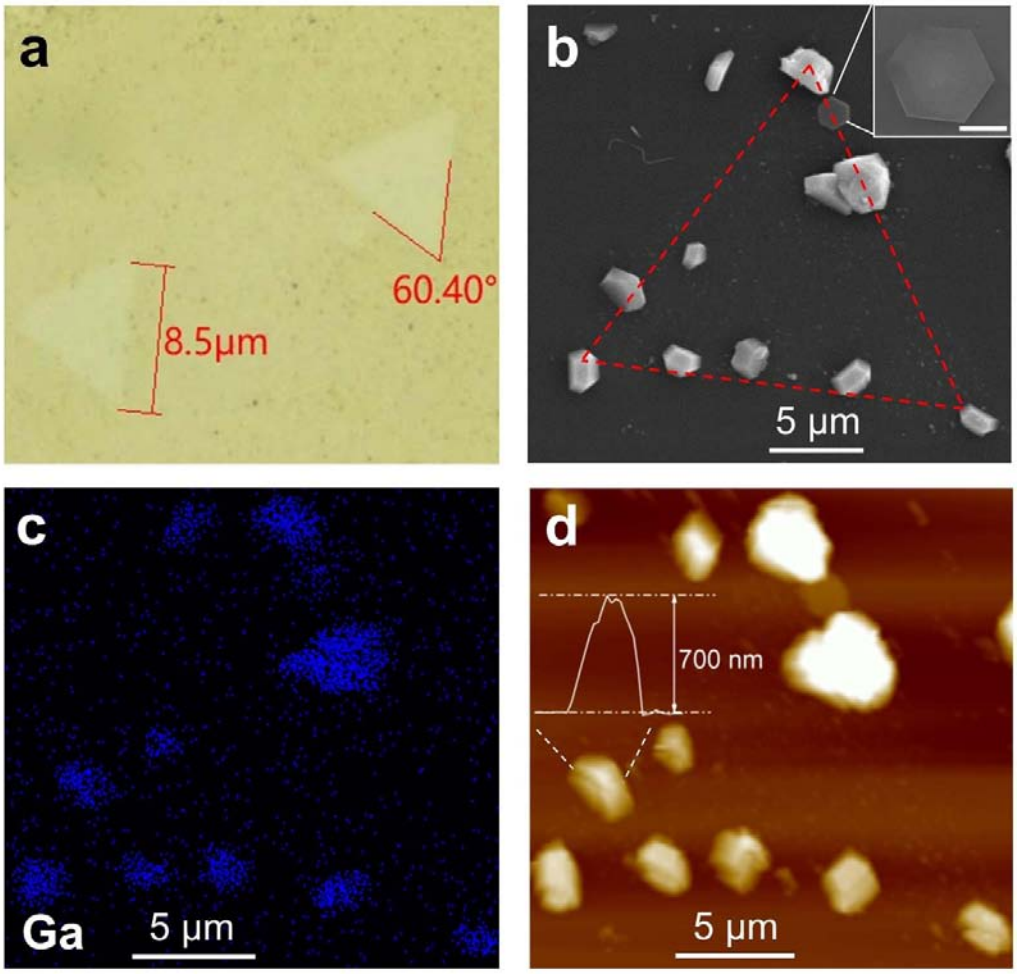

Figure 3. Growth of GaN islands on monocrystal h-BN triangles. (a) Optical image of monocrystalline triangular h-BNs on sapphire. (b) SEM of GaN nanocrystallines after a CVD growth process on anthe h-BN triangle substrate of figure 3(a). The inset shows a standard hexagonal GaN nanocrystallite. The scale bar is 1 μm. (c) EDS mapping of Ga elements corresponding to figure 3(b). (d) AFM height profile of GaN nanocrystallites corresponding to figure 3(b).

of GaN nanocrystallites on h-BN/sapphire, and the nanocrystallite height is about 700 nm. The above results indicate that GaN nanocrystallites preferentially grow on the edges of monocrystalline equilateral-triangle-shaped h-BNs. Some groups also reported that the edges of 2D material flakes are expected to have some structural imperfections which have a high electron affinity that could act as active nucleation centers for epitaxial growth [33, 34]. To further prove this idea, the adsorption and nucleation of Ga atoms on h-BN have been calculated using DFT. We constructed standard monolayer h-BN nanobelt structures without grain boundaries but with different edge-cut directions, as shown in the armchair pattern in figure 4(a) and the zigzag pattern in figure 4(b) [35]. Sites 1 and 4 mean that Ga atoms are attached to the edge (armchair edge and zigzag edge) of monocrystalline h-BN, while sites 2 and 3 mean the interior. The Ga atomic adsorption energy at different sites has been calculated in figure 4(c). The adsorption energies are calculated by

$$E_a = E_{\text{total}} - E_{\text{slab}} - E_{\text{Ga}}$$

where E_{total} is the total energy of the adsorbed system, E_{slab} is the total energy of the slab model, and E_{Ga} is the energy of a single Ga atom. The relative energies at the edge (sites 1 and 4) are about 2.1 ~ 4.3 eV and 1.7 eV lower than in the interior (sites 2 and 3) for the zigzag and armchair patterns, respectively. Thus, a Ga atom can more easily be adsorbed on the edge of monocrystalline trianglular h-BN than in the interior. Many experimental and theoretical calculations indicate that the edges of triangular h-BN form a zigzag pattern and are nitrogen-terminated (figure 4(d)) [36–39]. In addition, 2D materials can relax the strict requirements of conventional heteroepitaxy utilizing the QvdWE method [6, 9, 21–25]. Thus, a possible GaN island nucleation model at the edge of the monocrystalline triangluar h-BN is proposed in figure 4(e). The model shows that the Ga atoms are bonded to N atoms on the edge of the triangular h-BN by QvdWE. However, the in-plane lattice parameters are 0.250 nm for h-BN and 0.319 nm for hexagonal wurtzite GaN [39, 40], showing a large lattice mismatch of 27.4%. The calculation shows that every 4 unit cells of h-BN and every 3 unit cells of GaN have a coincidence with a small misfit of only 4.5%. Thus, we suspect that

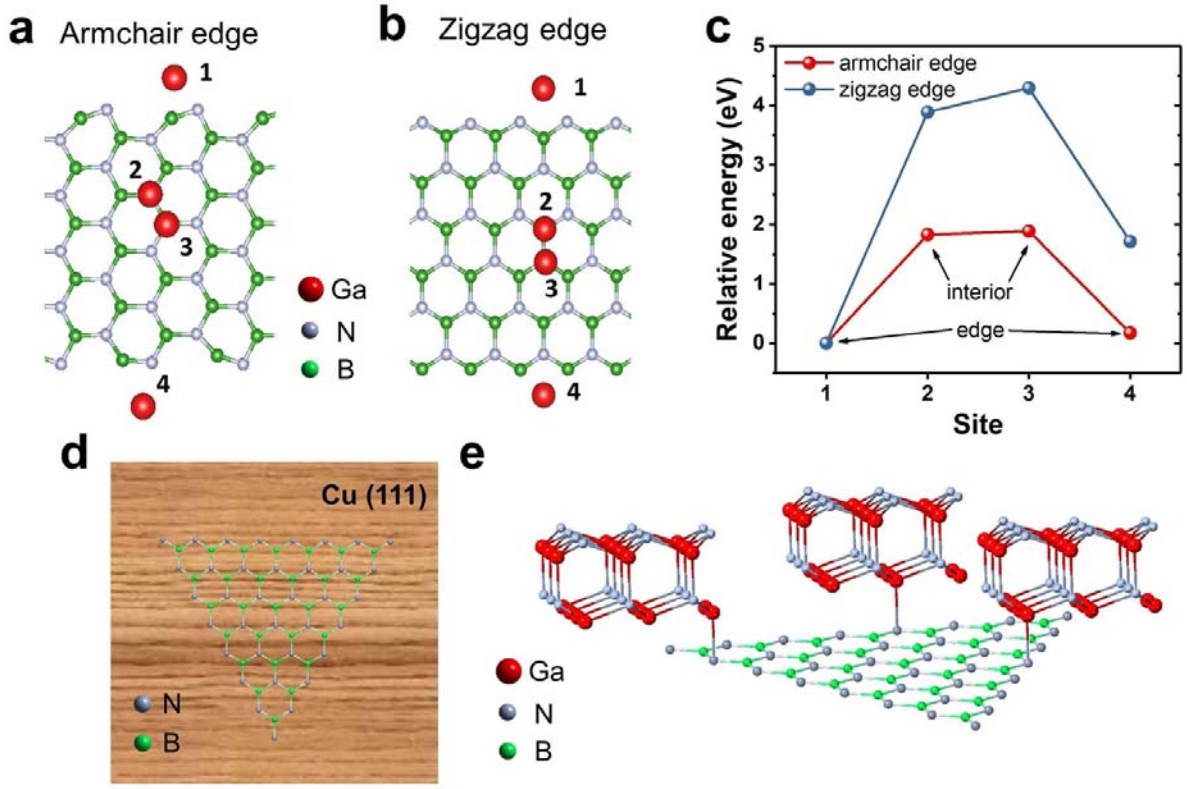

Figure 4. Grown molecule model and computational model of GaN on h-BN. (a, b) Model of Ga adsorbed on different sites of h-BN with armchair edge and zigzag edge. (c) Total relative energy of Ga adsorbed on different sites of h-BN. (d) Schematic illustration of monocrystalline triangular h-BN on Cu (111). (e) Epitaxial model of GaN islands on the edge of monocrystalline triangular h-BN.

for every 3 unit cells of GaN, epitaxial growth can be realized on 4 unit cells of h-BN. A similar epitaxial growth mode has been proposed by Kumaresan *et al* to explain GaN growth on a graphene substrate [40].

The vapor-solid (VS) mechanism will further control the growth of GaN nanocrystallites utilizing the CVD technology, which causes growth in multiple directions and various shapes [41–43]. Following CVD, the GaN nanocrystallines grow and finally merge into continuous films, as shown in figures 1(c) and S5. The thickness of the GaN film increases with increasing growth time. This causes squeezing and twisting in continuous GaN films due to the merging process. Herein, the test results of XRD and Raman spectroscopy imply the existence of the merging process. First of all, compared to the GaN nanocrystallites, other GaN wurtzite crystal peaks appear, including ((110), (200), (112), (201) and (202)) in the continuous GaN films shown in figure S4. Secondly, Raman peaks appear, located at 142.47 cm^{-1} and 533.02 cm^{-1} corresponding to wurtzite GaN E_2^{low} and an A_1(TO) mode in figure 2(d), which are not allowed by the Raman selection rules in the $(z(-,-)\bar{z})$ geometry [29, 44].

Furthermore, 150 min-grown continuous GaN film was used to fabricate the UV PD. A schematic diagram and an optical image are shown in figure 5(a) and the inset of figure 5(b), respectively. Figure 5(b) shows current—voltage (I–V) curves in the dark and under UV light illumination with a series of wavelengths (300 nm, 325 nm, 350 nm, 360 nm, and 375 nm). The time-dependent photon response ($\Delta I = I_{photo} - I_{dark}$) is further investigated under various wavelengths of illumination, as shown in figure 5(c). Herein, the light (300 nm, 325 nm, 350 nm, 375 nm, and 400 nm) is switched on and off sequentially, at a bias of 1.7 V. The response curve can be fitted with a bi-exponential relaxation equation, with relaxation times under 360 nm light in the decay stage of $\tau_1 \approx 54$ s and $\tau_2 \approx 388$ s. The existence of grain boundary defects in the merged GaN film should be the cause of the long relaxation time. The maximum responsivity at the band edge position is 0.57 A W^{-1} under 360 nm illumination, with a 6.34 mW cm^{-2} power density at 2 V of bias, as shown in figure 5(d). At the same time, there is a sharp cutoff wavelength above 360 nm approximatively corresponding to the GaN bandgap energy of 3.4 eV. Figure 5(e) shows the time-dependent photoresponse under 360 nm illumination at bias volatages of 1 V, 1.5 V, and 2 V. Figure 5(f) illustrates the variation in responsivity and external quantum efficiency (EQE) under 360 nm illumination with different applied bias voltages. There is a significant increase in responsivity from 0 to 0.57 A W^{-1} with an increasing bias from 0 to 2 V, respectively. The EQE increases with increasing applied voltage and reaches 1.94 (194%) at 2 V. Compared with some reported GaN-based PDs listed in table 1, our current CVD-grown GaN-based device shows a relatively high responsivity.

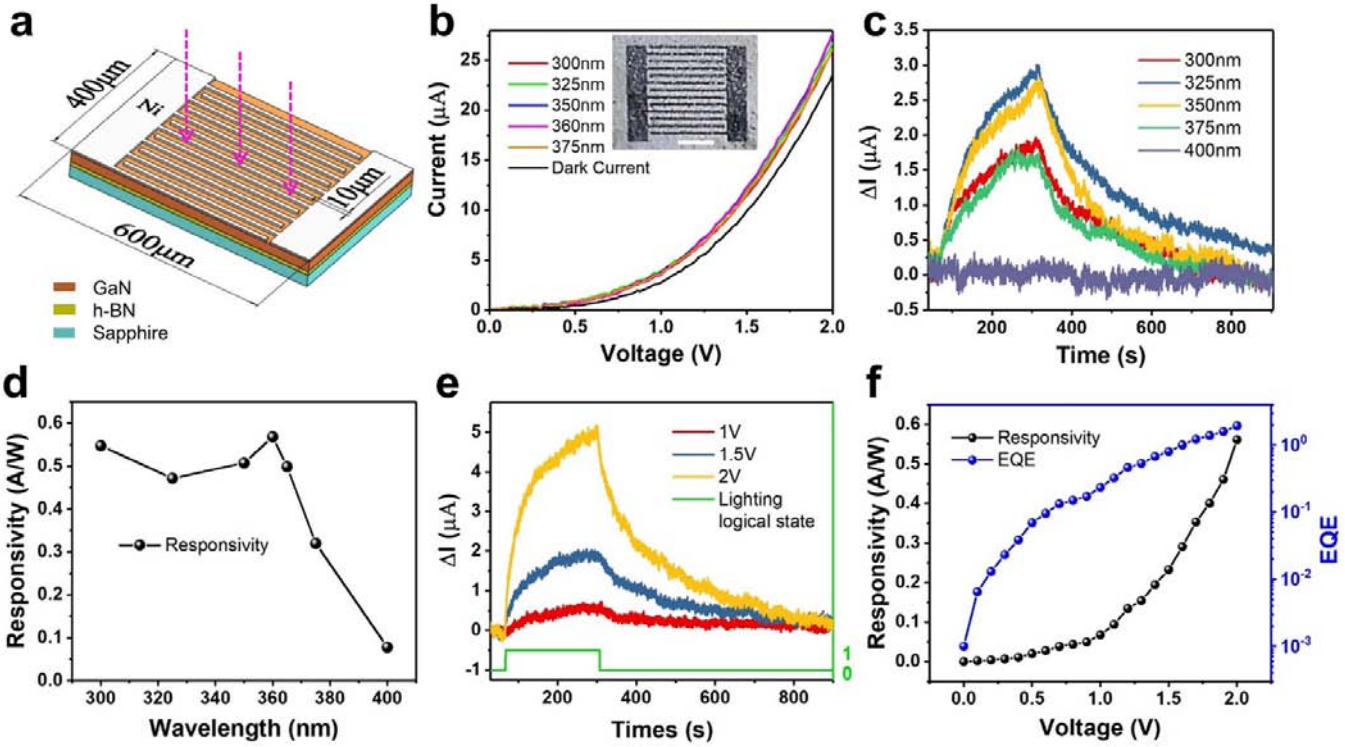

Figure 5. The detection performance of GaN-based photodetectors. (a) Schematic diagram of GaN-based metal-semicondctor-metal (MSM) photodetector. (b) *I*-*V* curves measured in the dark and at under illumination at different light wavelengths. The inset shows an optical image of the photodetector, the scale bar is 200 nm. (c) Time-dependent photoresponse at under illumination underby different light wavelengths at 1.7 V of bias. (d) Responsivity of GaN-based photodetector at different wavelengths at 2 V of bias. (e) Time-dependent photoresponse with varying bias under illumination by 360 nm light. (f) Variation in responsivity and EQE with bias voltages from 0 V to 2 V.

Table 1. Comparison of critical parameters in various GaN photodetectors.

Device structure	Fabrication method	Light of detection	Dark current	Responsivity	Relaxation time	Reference
GaN MSM	MOCVD	300–380 nm	10 pA at 1 V	50–150 A W^{-1} at 6–15 V	/	[45]
GaN MSM	MBE	254 302 365 nm	13 nA at 2 V	0.354 A W^{-1} at 2 V	/	[46]
GaN	MOCVD	300–360 nm	10 pA at − 1 V	0.11 A W^{-1} at −1 V	430 ns	[47]
GaN MSM	Thermal vapor deposition	365 nm	6.13 μA at 5 V	0.285 A W^{-1} at 5 V	10.4 ms	[32]
GaN MSM	MOCVD	362 nm	200 pA at 3 V	0.05 A W^{-1} at 5 V	/	[48]
GaN MSM	HVPE	365 nm	2 pA at 10 V	0.6 A W^{-1} at 5 V	/	[49]
GaN MSM	PAMBE	325 nm	1.5 μA at 5 V	0.320 A W^{-1} at 5 V	450 ms	[2]
GaN on graphene MSM	MOCVD	340–370 nm	9 μA at 0.5 V	2.5 A W^{-1} at 0.5 V	>500 s	[50]
GaN on h-BN MSM	CVD	300–360 nm	23 μA at 2 V	0.57 A W^{-1} at 2 V	$\tau_1 \approx 54s$ $\tau_2 \approx 388s$	This work

4. Conclusions

In conclusion, a continuous GaN film was realized on a sapphire substrate with a monolayer h-BN insertion layer using a simple CVD approach. By adjusting the growth time, we have accomplished growth from GaN islands to continuous film. The CVD growth mechanism with a specific h-BN insertion layer was investigated with experiments and quantitative theoretical calculation. The results indicate that GaN nanocrystallites are preferentially formed at the edges of monocrystalline triangular h-BN by QvdWE. Many of GaN nanocrystallites will subsequently grow and merge into a continuous film by the VS mechanism. In addition, the UV PD based on the CVD-grown continuous GaN film shows a satisfactory detection performance. Further work will focus on improving the crystal quality by optimizing the CVD growth process. Our work offers a simple, complementary, and alternative method for the growth of GaN films, thereby promoting their wide application.

Acknowledgments

This work was supported by the National Key Research and Development Program of China (Grant No. 2018YFB0406702), the Natural science foundation of Hunan province, China (Grant No. 2019JJ50751), the Project of the State Key Laboratory of High-Performance Complex Manufacturing, Central South University, China (Grant Nos. ZZYJKT2019-13 and ZZYJKT2018-01), the start-up funding (Grant Nos. 218091 and 217056).

Conflicts of interest

There are no conflicts to declare.

ORCID iDs

Wenhui Zhu https://orcid.org/0000-0002-4889-781X
Lei Zhang https://orcid.org/0000-0001-7101-4619

References

[1] Feng Y *et al* 2019 Epitaxy of single-crystalline GaN film on CMOS-compatible Si(100) Substrate buffered by graphene *Adv. Funct. Mater.* **29** 1–7
[2] Gundimeda A, Krishna S, Aggarwal N, Sharma A, Sharma N D, Maurya K K, Husale S and Gupta G 2017 Fabrication of non-polar GaN based highly responsive and fast UV photodetector *Appl. Phys. Lett.* **110** 1–4
[3] Miller R A, Cruden B A, Martinez R and Senesky D G 2017 *In situ* ultraviolet shock radiance measurements using GaN-on-sapphire photodetectors *Rev. Sci. Instrum.* **88** 1–7
[4] Kou J, Shen -C-C, Shao H, Che J, Hou X, Chu C, Tian K, Zhang Y, Zhang Z-H and Kuo H-C 2019 Impact of the surface recombination on InGaN/GaN-based blue micro-light emitting diodes *Opt. Express* **27** A643–53
[5] Wang L, Liu Z, Li Z, Zhang Y, Li H, Yi X, Wang J, Wang G and Li J 2017 Nanostructure nitride light emitting diodes via the Talbot effect using improved colloidal photolithography *Nanoscale* **9** 7021–6
[6] Kobayashi Y, Kumakura K, Akasaka T and Makimoto T 2012 Layered boron nitride as a release layer for mechanical transfer of GaN-based devices *Nature* **484** 223–7
[7] Chung K, Lee C H and Yi G C 2010 Transferable GaN layers grown on ZnO-coated graphene layers for optoelectronic devices *Science* **330** 655–7
[8] Andre Y, Trassoudaine A, Tourret J, Cadoret R, Gil E, Castelluci D, Aoude O and Disseix P 2007 Low dislocation density high-quality thick hydride vapour phase epitaxy (HVPE) GaN layers *J. Cryst. Growth* **306** 86–93
[9] Zhang L *et al* 2015 Improving the quality of GaN crystals by using graphene or hexagonal boron nitride nanosheets substrate *ACS Appl. Mater. Interfaces* **7** 4504–10
[10] Tamura K, Kuroki Y, Yasui K, Suemitsu M, Ito T, Endou T, Nakazawa H, Narita Y, Takata M and Akahane T 2008 Growth of GaN on SiC/Si substrates using AlN buffer layer by hot-mesh CVD *Thin Solid Films* **516** 659–62
[11] Yang S H, Ahn S H, Jeong M S, Nahm K S, Suh E K and Lim K Y 2000 Structural and optical properties of GaN films grown by the direct reaction of Ga and NH3 in a CVD reactor *Solid State Electron.* **44** 1655–61
[12] Song W, Si J, Wu S, Hu Z, Long L, Li T, Gao X, Zhang L, Zhu W and Wang L 2019 Synthesis and morphology evolution of indium nitride (InN) nanotubes and nanobelts by chemical vapor deposition *Cryst. Eng. Comm.* **21** 5356–62
[13] Wu S *et al* 2018 Ultrafast growth of horizontal GaN nanowires by HVPE through flipping the substrate *Nanoscale* **10** 5888–96
[14] Wang Y-Q, Wang R-Z, Li Y-J, Zhang Y-F, Zhu M-K, Wang -B-B and Yan H 2013 From powder to nanowire: a simple and environmentally friendly strategy for optical and electrical GaN nanowire films *Cryst. Eng. Comm.* **15** 1626–34
[15] Liang D, Wei T, Wang J and Li J 2020 Quasi van der Waals epitaxy nitride materials and devices on two dimension materials *Nano Energy* **69** 104463
[16] Kong W *et al* 2018 Polarity governs atomic interaction through two-dimensional materials *Nat. Mater.* **17** 999–1004
[17] Bae S H, Kum H, Kong W, Kim Y, Choi C, Lee B, Lin P, Park Y and Kim J 2019 Integration of bulk materials with two-dimensional materials for physical coupling and applications *Nat. Mater.* **18** 550–60
[18] Bae S-H *et al* 2020 Graphene-assisted spontaneous relaxation towards dislocation-free heteroepitaxy *Nat. Nanotechnol.* **15** 272-276
[19] Susanto I, Tsai C-Y, Fachruddin , Rahmiati T, Ho Y-T, Tsai P-Y and Yu I-S 2019 The influence of 2D MoS2 layers on the growth of GaN films by plasma-assisted molecular beam epitaxy *Appl. Surf. Sci.* **496** 143616
[20] Wu Q *et al* 2017 Growth mechanism of AlN on hexagonal BN/sapphire substrate by metal–organic chemical vapor deposition *Cryst. Eng. Comm.* **19** 5849–56
[21] Chen Z *et al* 2019 Improved epitaxy of AlN film for deep-ultraviolet light-emitting diodes enabled by graphene *Adv. Mater.* **31** 1–8
[22] Li T, Liu C, Zhang Z, Yu B, Dong H, Jia W, Jia Z, Yu C, Gan L and Xu B 2018 GaN epitaxial layers grown on multilayer graphene by MOCVD *AIP Adv.* **8** 1–6
[23] Kim J, Bayram C, Park H, Cheng C W, Dimitrakopoulos C, Ott J A, Reuter K B, Bedell S W and Sadana D K 2014 Principle of direct van der Waals epitaxy of single-crystalline films on epitaxial graphene *Nat. Commun.* **5** 1–7
[24] Kim Y *et al* 2017 Remote epitaxy through graphene enables two-dimensional material-based layer transfer *Nature* **544** 340–3
[25] Mun D-H, Bae H, Bae S, Lee H, Ha J-S and Lee S 2014 Stress relaxation of GaN microstructures on a graphene-buffered Al2O3substrate *Phys. Status Solidi RRL* **8** 341–4
[26] Kresse G, Furthmuller J and Hafner J 1994 Theory of the crystal structures of selenium and tellurium: the effect of generalized-gradient corrections to the local-density approximation *Phys. Rev.* B **50** 13181–5
[27] Perdew J P, Burke K and Ernzerhof M 1998 Perdew, Burke, and Ernzerhof reply *Phys. Rev. Lett.* **80** 891–891
[28] Tang J, Liang T, Shi W, Zhang Q, Wang Y, Liu J and Xiong J 2011 The testing of stress-sensitivity in heteroepitaxy GaN/Si by Raman spectroscopy *Appl. Surf. Sci.* **257** 8846–9
[29] Hushur A, Manghnani M H and Narayan J 2009 Raman studies of GaN/sapphire thin film heterostructures *J. Appl. Phys.* **106** 1–5
[30] Luo S, Fan J, Liu W, Zhang M, Song Z, Lin C, Wu X and Chu P K 2006 Synthesis and low-temperature photoluminescence properties of SnO_2 nanowires and nanobelts *Nanotechnology* **17** 1695–9

[31] Khan N and Li J 2006 Effects of compressive strain on optical properties of InxGa1−xN/GaN quantum wells *Appl. Phys. Lett.* **89** 15
[32] Saron K M A, Hashim M R and Farrukh M A 2013 Growth of GaN films on silicon (111) by thermal vapor deposition method: optical functions and MSM UV photodetector applications *Superlattices Microstruct.* **64** 88–97
[33] Qin J K *et al* 2018 Epitaxial growth of 1D atomic chain based Se nanoplates on monolayer ReS_2 for high-performance photodetectors *Adv. Funct. Mater.* **28** 1–8
[34] Kim M S, Yun S J, Lee Y, Seo C, Han G H, Kim K K, Lee Y H and Kim J 2016 Biexciton emission from edges and grain boundaries of triangular WS(2) monolayers *ACS Nano* **10** 2399–405
[35] Liu Y, Bhowmick S and Yakobson B I 2011 BN white graphene with 'colorful' edges: the energies and morphology *Nano Lett.* **11** 3113–6
[36] Kim K K *et al* 2012 Synthesis of monolayer hexagonal boron nitride on Cu foil using chemical vapor deposition *Nano Lett.* **12** 161–6
[37] Auwärter W, Muntwiler M, Osterwalder J and Greber T 2003 Defect lines and two-domain structure of hexagonal boron nitride films on Ni(111) *Surf. Sci.* **545** L735–L740
[38] Auwärter W, Suter H U, Sachdev H and Greber T 2004 Synthesis of one Monolayer of hexagonal boron nitride on Ni(111) from B-trichloroborazine (ClBNH)3 *Chem. Mater.* **16** 343–5
[39] Li Q, Zou X, Liu M, Sun J, Gao Y, Qi Y, Zhou X, Yakobson B I, Zhang Y and Liu Z 2015 Grain boundary structures and electronic properties of hexagonal boron nitride on Cu(111) *Nano Lett.* **15** 5804–10
[40] Kumaresan V *et al* 2016 Epitaxy of GaN nanowires on graphene *Nano Lett.* **16** 4895–902
[41] Jindal V and Shahedipour-Sandvik F 2009 Theoretical prediction of GaN nanostructure equilibrium and nonequilibrium shapes *J. Appl. Phys.* **106** 8
[42] Li H, Geelhaar L, Riechert H and Draxl C 2015 Computing equilibrium Shapes of wurtzite crystals: the example of GaN *Phys. Rev. Lett.* **115** 085503
[43] Carvajal J, Gomez N, Bai J, Dudley M and Rojo J 2006 Synthesis of nanoporous GaN crystalline particles by chemical vapor deposition - art. no. 61210E *Proc. SPIE Int. Soc. Opt. Eng.* **6121** 61210E
[44] Harima H 2002 Properties of GaN and related compounds studied by means of Raman scattering *J. Phys.: Condens. Matter* **14** R967–R993
[45] Müller A *et al* 2009 GaN membrane-supported UV photodetectors manufactured using nanolithographic processes *Microelectron. J.* **40** 319–21
[46] Velazquez R, Aldalbahi A, Rivera M and Feng P 2016 Fabrications and application of single crystalline GaN for high-performance deep UV photodetectors *AIP Adv.* **6** 1–12
[47] Yagi S 2000 Highly sensitive ultraviolet photodetectors based on Mg-doped hydrogenated GaN films grown at 380 °C *Appl. Phys. Lett.* **76** 345–7
[48] Zhao M, Bao J, Fan X, Gu F, Guo Y, Zhang Y, Zhao M, Sha Y, Guo F and Li J 2009 Effects of thermal annealing on the properties of GaN MSM UV photodetectors *Phys.* B **404** 275–7
[49] Xie F, Lu H, Xiu X, Chen D, Han P, Zhang R and Zheng Y 2011 Low dark current and internal gain mechanism of GaN MSM photodetectors fabricated on bulk GaN substrate *Solid State Electron.* **57** 39–42
[50] Journot T, Bouchiat V, Gayral B, Dijon J and Hyot B 2018 Self-assembled UV photodetector made by direct epitaxial GaN growth on graphene *ACS Appl. Mater. Interfaces* **10** 18857–62